Journal of Molecular Structure 1028 (2012) 116–125

Contents lists available at SciVerse ScienceDirect

Journal of Molecular Structure

journal homepage: www.elsevier.com/locate/molstruc

Synthesis, characterization and antimicrobial activity of *m*-toluenesulfonamide, *N*,*N*′-1,2-ethanediylbis (mtsen) and [Cu(II)(phenanthroline)$_2$]mtsen complex

Hamit Alyar [a], Saliha Alyar [b,*], Arslan Ünal [c], Neslihan Özbek [d], Ertan Şahin [e], Nurcan Karacan [f]

[a] Department of Chemistry, Science Faculty, Çankırı Karatekin University, 18100 Çankırı, Turkey
[b] Department of Physics, Science Faculty, Çankırı Karatekin University, 18100 Çankırı, Turkey
[c] Department of Physics, Science and Art Faculty, Bilecik University, 11210 Bilecik, Turkey
[d] Department of Primary Education, Faculty of Education, Ahi Evran University, 40100 Kırşehir, Turkey
[e] Department of Chemistry, Faculty of Science and Art, Atatürk University, TR-25240 Erzurum, Turkey
[f] Department of Chemistry, Science and Art Faculty, Gazi University, 06500 Ankara, Turkey

HIGHLIGHTS

- *M*-toluenesulfonamide, *N*,*N*′-1,2-ethanediylbis (mtsen) and [Cu(II)(phenanthroline)$_2$]mtsen compounds were synthesized.
- The structure of msen was proved by single-crystal X-ray diffraction, spectral analyses and DFT.
- The structure of complex was investigated magnetic susceptibility, conductivity measurement and FT-IR.
- The complete assignments of mtsen were performed on the basis of the PED.
- The in-vitro antibacterial activities of compounds were also tested.

ARTICLE INFO

Article history:
Received 23 February 2012
Received in revised form 22 June 2012
Accepted 22 June 2012
Available online 29 June 2012

Keywords:
Disulfonamides
X-ray
DFT
SQM-FF
FT-IR and Raman
Antibacterial activity

ABSTRACT

M-toluenesulfonamide, *N*,*N*′-1,2-ethanediylbis (a disulfonamide compound, mtsen) and [Cu(II)(phenanthroline)$_2$]mtsen compounds were newly synthesized. The molecular structure of mtsen was investigated by using elemental analyses, liquid chromatography–mass spectrometry (LC–MS), X-ray diffraction, Fourier transform infrared spectroscopy (FT-IR), dispersive Raman spectroscopy, ^{1}H, ^{13}C, heteronuclear chemical-shift correlation (HETCOR) and correlation spectroscopy (COSY) NMR spectroscopies. The FT-IR, dispersive Raman and far-infrared spectra of mtsen were recorded at room-temperature and discussed assisted with B3LYP/6-311G(d,p) level of theory along with scaled quantum mechanics force field (SQM-FF) method. Furthermore, ^{1}H and ^{13}C NMR analyses were performed at B3LYP/6-311++G(d,p) theory level using gauge including atomic orbital (GIAO) method and compared with the experimental findings. Further analyses were also made for [Cu(II)(phenanthroline)$_2$]mtsen complex by using elemental analysis, LC–MS, magnetic susceptibility; conductivity measurement and FT-IR. The antibacterial activities of synthesized compounds were studied against some Gram-positive and Gram-negative bacteria by using the microdilution and disk diffusion method. The biological activity screening showed that complex have more activity than ligand against the tested bacteria.

1. Introduction

Sulfa drugs are the oldest chemically synthesized antimicrobial agents and are still widely used today for the treatment of various bacterial, protozoal and fungal infections [1,2]. After the introduction of the penicillin and other antibiotics the popularity of sulfonamides decreased. However they are still used as sulfa drugs such as sulfadiazine, sulfathiazole and sulfamerazine in certain therapeutic fields especially in the case of ophthalmic infections and for urinary and gastrointestinal infections [3,4]. Multidrug resistance remains as a significant problem for microbial infection treatments [5–8]. Additionally the threat of bioterrorism using agents such as weaponized *Bacillus* anthracis and *Yersinia* pestis highlight the need for continuing research in infectious diseases and the search for new therapeutic agents [9]. Due to their significant pharmacology applications and widespread use in medicine, these compounds have gained attention in bio-inorganic and metal-based drug chemistry.

Some metal sulfonamide complexes have attracted much attention due to the fact that showing greater biological activity than the sulfonamide ligands or the metallic salts. For instance,

* Corresponding author. Tel.: +90 0376 2132626.
E-mail address: saliha@karatekin.edu.tr (S. Alyar).

0022-2860/$ - see front matter © 2012 Elsevier B.V. All rights reserved.
http://dx.doi.org/10.1016/j.molstruc.2012.06.046

Ag(I)-sulfadiazine [10], Ce(III)-sulfadiazine [11], Ni(II)-sulfadimethoxine [12] and Cu(II)-sulfacetamide [13] have shown higher antimicrobial activity than free ligands.

In our previous studies, some aliphatic or aromatic bis sulfonamide compounds were synthesized and their antimicrobial activity were tested [14–17]. Furthermore, we have reported conformational analysis and vibrational spectroscopic investigation of the methanesulfonic acid hydrazide [18], methanesulfonic acid 1-methylhydrazide [19], some methanesulfonyl hydrazone derivatives [20–22]. We also reported the conformational behavior, vibrational and NMR spectroscopic study of methanesulfonamide-*N*,*N*′-1,2-ethanediylbis (msen) in our last study [23]. As a continuation our studies, the aims of the current work is to interpret the molecular structure, vibrational and NMR spectroscopic properties of the mtsen from experimental and theoretical viewpoints as a contribution to the understanding of the rational drug design of sulfonamide derivatives. Furthermore, $[Cu(phen)_2]L$ complex (where Cu(II)=Cu, phen = phenanthroline and L = mtsen) was synthesized and characterized by using elemental analyses, FT-IR, LC–MS, magnetic susceptibility and conductivity measurements. Finally, the antibacterial activities of synthesized two compounds were investigated by using disk diffusion and micro dilution methods.

2. Experimental and theoretical part

2.1. Synthesis of ligand molecule

The nucleophilic substitution reaction of the 1,2 diaminopropane with *m*-toluenesulfonyl chloride were carried out as follows: tetrahydrofuran solution of 1,2 diaminopropane (0.08 mol, 3.36 mL) was added by slowly dropwise to the tetrahydrofuran solution of *m*-toluenesulfonyl chloride (0.04 mol, 3.85 g), maintaining the temperature between −5 and −10 °C. Then, the reaction mixture was stirred for 24 h at room temperature (completion of the reaction was monitored by thin layer chromatography). After the completion of the reaction, the solvent was evaporated in vacuum. The solid residue was purified by column chromatography. The white crystalline solid was recrystallized from tetrahydrofuran/*n*-hexane mixture. Product was dried in a vacuo and stored at tetrahydrofuran vapor. Yield 72%; mp 158–161 °C MS (70 eV, APCl): 368.8 (M^+), 369.8 (M^{1+}), 370.8 (M^{2+}), 214.7 ($CH_3C_6H_4SO_2NHC_2H_4NH^+$), 167.6 $(CH_3C_6H_4SO_2NH)^+$ 154.6 $(CH_3C_6H_4SO_2)^+$. Anal. Calc. for $C_{16}H_{20}N_2O_4S_2$: C, 40.0; H 8.0; N, 9.33; S, 21.3. Found: C, 40.23; H, 7.94; N, 9.10; S, 21.51.

2.2. Synthesis of $[Cu(phen)_2]L$ complex

0.5 mmol of *m*-toluenesulfonamide, *N*,*N*′-1,2-ethanediylbis was added to a solution of 0.5 mmol of Cu(II) acetate in 40 ml of acetonitrile. The mixture was stirred for 3–4 h. Then, 1 mmol of 1,10-phenanthroline was added into the mixture. Product precipitated slowly as a blue solid while the mixture was warmed. The product was filtered off, dried, and recrystallized from dichloromethane/*n*-hexane. Data for $[Cu(phen)_2]L$ (phen: phenanthroline and L:mtsen) complex (yield 70%). mp 338–340 °C MS (70 eV, APCl): 790 $[CuL(phen)_2]^+$, 425.0 $[Cu(phen)_2]^+$ 243.9 $[Cu(phen)]^+$, 368 $[HL1]^+$. Anal. Calc. for $C_{40}H_{34}N_6O_4S_2Cu$: C, 61.22; H, 4.51; N, 10.45; S, 7.97. Found: C, 58.99; H, 4.51; N, 12.58; S, 4.85.

2.3. Physical measurements

The elemental analyses (C, H, N and S) were performed by a Fisons EA-108 type elemental analyzer. The mass spectrum was recorded on Agilent 1100 LC/MS-APCI at 100 eV. Thin layer chromatography (TLC) was conducted on 0.25 mm silica gel plates (60F254, Merck). All NMR spectra were recorded on a Bruker WM-400 spectrometer at ambient probe temperature using dimethyl sulfoxide-d_6 (DMSO-d_6) solutions with tetramethylsilane as internal reference. The FT-IR (4000–400 cm^{-1}) spectra between KBr pellet technique or KBr windows as Nujol or hexachloro-1,3-butadiene mulls and far-infrared (400–30 cm^{-1}) spectra between polyethylene pellet technique of the sample were recorded by using a Bruker Optics IFS66v/s FTIR spectrometer with 2 cm^{-1} resolution in vacuum. The dispersive Raman spectra were recorded using a Bruker Senterra Dispersive Raman microscope spectrometer at 532 nm excitation from a doubled Nd/YAG laser having 3 cm^{-1} resolution between 4000 and 100 cm^{-1} spectral region. The molar magnetic susceptibilities at room temperature were performed using a Sherwood Scientific Magway MSB MK1 model magnetic balance by the Gouy method using $Hg[Co(SCN)_4]$ as the calibrant measurement. The molar conductance measurements were carried out using a Siemens WPA CM 35 conductometer.

2.4. Computational details

The geometric parameters of mtsen were fully optimized without any constraint with the help of standard gradient procedure implemented within Gaussian 03 program [24]. All the parameters were allowed to relax and all the calculations converged to an optimized geometry which corresponds to a true energy minimum revealed by the lack of imaginary values in the wave numbers calculations. The vibrational wavenumbers were calculated with B3LYP/6-311G(d,p) and then scaled by using the scaling factors for primitive coordinates proposed by our previous study [23]. The scale factor values used in the SQM-FF methodology for internal coordinates are given Table S1 (Supporting information). The each vibrational modes of the studied compound were characterized by their potential energy distributions (PED) which were calculated by using SQM-FF program [25].

The scaling factors were not applied to the infrared and Raman intensities. The relative Raman intensity (I^R), which simulates the measured Raman spectrum, was calculated using the following relation derived from the intensity theory of Raman scattering [26,27];

$$I_i^R = \frac{f(\nu_0 - \nu_i)^4 S_i}{\nu_i[1 - \exp(-hc\nu_i/kT)]} \tag{1}$$

where ν_0 is the exciting frequency (18798 cm^{-1}), ν_i is the vibrational wavenumber of the *i*th normal mode (in cm^{-1} units), S_i is the Raman scattering activity of the *i*th normal mode q_i, h, c, k are fundamental constants, T = 300°K and f (10^{-14}) is a suitably chosen common normalization factor for all peaks.

NMR features of mtsen were calculated at B3LYP/6-311++G(d,p) theory level using GIAO method [28,29] as implemented in Gaussian 03W program package. Isotropic shielding tensors of ^{13}C and ^{1}H were turned into chemical shifts using the linear relationship equation as in Ref. [23].

2.5. Crystal structure of the mtsen

To get the molecular structural parameters of mtsen, the single-crystal of the compound was used for data collection on a four-circle Rigaku R-AXIS RAPID-S diffractometer (equipped with a two-dimensional area IP detector). The graphite-monochromatized Mo $K\alpha$ radiation (λ = 0.71073 Å) and oscillation scans technique with $\Delta\omega$ = 5° for one image were used for data collection. The lattice parameters were determined by the least-squares methods on the basis of all reflections with $F^2 > 2\sigma(F^2)$. Integration of the intensities, correction for Lorentz and polarization effects and cell refinement were performed using Crystal Clear (Rigaku/MSC Inc.,

Table 1
Crystal data and structure refinement parameters for mtsen.

CCDC number	861029	
Empirical formula	$C_{16}H_{20}N_2O_4S_2$	
Formula weight	368.4	
Temperature	293(2) K	
Wavelength	0.71073 Å	
Crystal system	Monoclinic	
Space group	$P2_1/c$	
Unit cell dimensions	a = 9.1034(2) Å	α = 90°
	b = 10.2851(2) Å	β = 114.41(3)°
	c = 10.1651(2) Å	γ = 90°
Volume	866.69(3) $Å^3$	
Z	2	
Density (calculated)	1.42 g/cm^3	
Absorption coefficient	0.330 mm^{-1}	
$F(000)$	388	
θ-range for data collection	2.5–30.7°	
Index ranges	$-13 \leq h \leq 13$, $-14 \leq k \leq 14$, $-14 \leq l \leq 13$	
Reflections collected	25110	
Independent reflections	2654 [R_{int} = 0.044]	
Completeness to θ = 30.7°	99.7%	
Refinement method	Full-matrix least-squares on F^2	
Data/restraints/parameters	2524/0/112	
Goodness-of-fit on F^2	1.143	
Final R indices [$F^2 > 2\sigma(F^2)$]	R_1 = 0.040, wR_2 = 0.119	
R indices (all data)	R_1 = 0.043, wR_2 = 0.124	
Extinction coefficient	0.080	
Largest diff. peak and hole	0.268 and −0.267 e $Å^{-3}$	

2005) software [30]. The structures were also solved by direct methods using SHELXS-97 and refined by a full-matrix least-squares procedure using the program SHELXL-97 [31]. All hydrogen atoms attached to carbon atoms were fixed geometrically and treated as riding with C—H = 0.97 Å (methylene) or 0.96 Å (methyl) with $U_{iso}(H) = 1.2U_{eq}$(methylene) and $1.5U_{eq}$(methyl) of the parent atom. The nitrogen protons were located in Fourier difference maps and constrained as riding atoms with N(1)—H(1 N) set to 0.950 Å. The final difference Fourier maps showed no peaks of chemical significance. Crystal data and structure refinement parameters of compound mtsen were tabulated in Table 1.

Crystallographic data were deposited in CSD under CCDC registration number 861029. These data can be obtained free of charge from The Cambridge Crystallographic Data Centre via www.ccdc.cam.ac.uk/data_request/cif.

2.6. Micro-dilution assays

Staphylococcus aureus ATCC 25923, *Bacillus cereus* RSKK 709, *Bacillus subtilis* ATCC 6633, *Escherichia coli* ATCC 35218, *Pseudomonas aeruginosa* ATCC 27853 and *Yersinia enterocolitica* O:3 cultures were obtained from the Department of Biology at Gazi University or the Refik Saydam Hygiene Center Culture Collection. Bacterial strains were cultured overnight at 37 °C in Nutrient Broth. These stock cultures were stored in the dark at 4 °C during the survey.

All tests were performed in a Nutrient Broth supplemented with DMSO to a final concentration of 10% (v/v) to enhance their solubility. Test strains were suspended in the Nutrient Broth by adjusting to the 0.5 McFarland standards. The compounds to be tested were dissolved in DMSO to give the highest concentration (450 μg mL^{-1}), and serial dilutions thereafter in sterile 10 mL test tubes containing nutrient broth to give sample concentrations of the range 45–450 μg mL^{-1}. The minimum inhibitory concentration (MIC) values of compounds were determined using a modification of the micro-well dilution assay method. 96 well plates were prepared by dispensing 95 μL of nutrient broth and 5 μL of the inoculums into each well. 100 μL from test compounds initially prepared at 450 μg mL^{-1} concentration were added into the first wells. Then, 100 μL from the serial dilutions was transferred into fourteen consecutive wells. The contents of the wells were mixed and the microplates were incubated at 37 °C for 24 h. The compounds were also tested against each microorganism twice. The MIC values were determined from visual examinations as the lowest concentration of the extracts in the wells with no bacterial growth [32].

2.7. Disk diffusion method

Bacterial susceptibility testing was performed by the disk diffusion method according to the guidelines of Clinical and Laboratory Standards Institute [33]. The sterilized (autoclaved at 120 °C for 30 min), liquefied Mueller Hinton agar (40–50 °C) was inoculated with the suspension of the microorganism (matched to 0.5 McFarland) and poured into a Petri dish to give a depth of 3–4 mm. The paper disks impregnated with the test compounds (50 μg, 100 μg and 250 μg) were placed on the solidified medium. Disks were placed on agar plates and the cultures were incubated at 37 °C for 24 h for bacteria. Inhibition zones formed on the medium were evaluated in mm. ciprofloxacin (5 μg/disk) was chosen as a standard in antibacterial activity measurements (positive control). DMSO poured disk was also used as negative control.

3. Results and discussion

3.1. The characterization of compounds

An X-ray diffraction analysis was undertaken to understanding the molecular structure of mtsen. The ORTEP diagram of mtsen is presented in Fig. 1. The compound crystallizes in the monoclinic space group *P21/c*, with two molecules in the unit cell. The structure has a 'partially extended' conformation in which the terminal *m*-toluenesulfonamide fragments fold back towards the diaminoethane unit. The molecule possesses crystallographically imposed centrosymmetry (Fig. 1). The crystal structure consists of layers where the sulfonamide atoms are involved in hydrogen bonding networks. As shown in Fig. 2, the sulfonamide group is involved in two hydrogen bonds (between O atoms of sulfonamide and nitrogen atoms) with symmetry-related molecules, building a two dimensional network parallel to the *bc*-plane [N1···$O1^i$ = 3.034(2), N1—H···$O1^i$ = 177°, Symmetry codes: (i) x,1/2 − y,1/2 + z]. N—H···O hydrogen bonding networks are the characteristic feature of other structural studies of the sulfonamides [34,35]. The methyl group was also allowed to rotate about its local threefold axis. One noticed that S═O of the sulfonyl unit bond lengths are a bit longer and also S—N and S—C bond lengths are shorter than in our previous structure [22].

Before offering an explanation for the molecular structure of $[Cu(phen)_2]L$ complex, the magnetic susceptibility and conductivity measurement were examined. The effective magnetic moment of the complex (as Bohr Magneton: B.M.) was measured at room

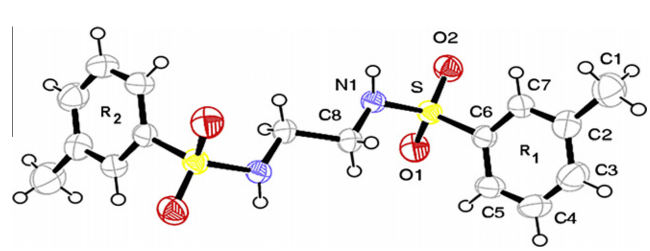

Fig. 1. The molecular structure of mtsen with the atom-numbering scheme; displacement ellipsoids are drawn at 40% probability level. The pairs of atoms C1/$C1^i$ etc. are related by the crystallographic inversion center.

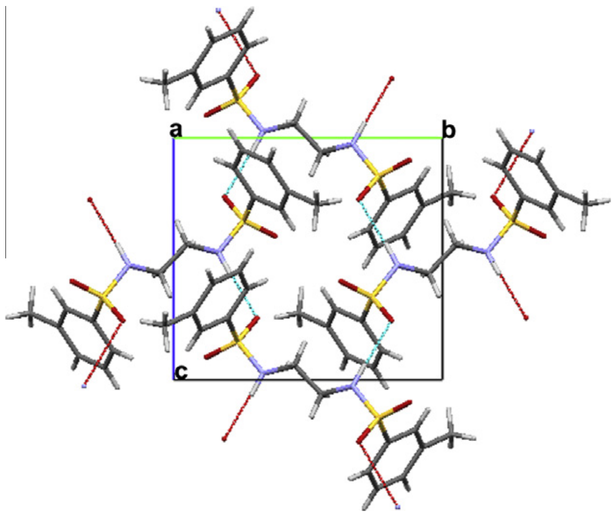

Fig. 2. Unit-cell packing diagram of mtsen.

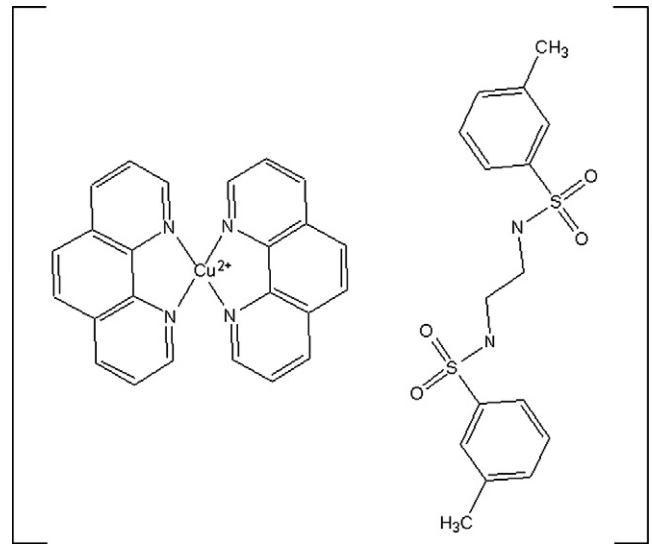

Fig. 3. The molecular structure of $[Cu(phen)_2]L$.

temperature. The magnetic moment of the complex (2.06 B.M.) is close to the spin value 1 for one unpaired electron and within the general range for Cu(II) complexes [36].

For the conductivity measurement of complex, the molar conductivity (Λ_m) of 10^{-3} M solution in DMSO of the complex was measured at 25 °C. The complex appears to be air stable, soluble in DMSO and slightly soluble in acetonitrile. The experimental conductivity value falls in the range of a 1:1 electrolyte [36,37]. Anionic ligand (L^{2-}) is bonded out of the coordination sphere as counter ion.

A lot number of Cu(II) complexes of related *N*-substituted sulfonamides have been reported [36–43]. Also, structural information about the deprotonated sulfonamide group conformation has been obtained too. The consequence of these studies offers that the copper atom is located on a twofold axis and is tetracoordinated by the four nitrogen atoms of two bidentate 1,10-phenanthroline molecules in $[Cu(phen)_2]^{++}$ cationic complex. Unusually, the sulfonamidate anions are not coordinated to Cu(II). Ligand does not interact with the metal ion and behaves as a counterion in complex.

From the results of related references, elemental analysis, mass spectrum, magnetic susceptibility, conductivity measurement as well as infrared spectrum (the interpretation is given after the vibrational spectral analysis of ligand), the molecular structure of $[Cu(phen)_2]L$ is presented in Fig. 3.

3.2. Geometry optimization results

The optimized geometric parameters (bond lengths, angles and torsion angles) calculated at B3LYP/6-311G(d,p) are listed with experimental findings form XRD results in Table 2. In general calculated geometric parameters seem to an agreement with experimental findings except S—N(1) bond length and S—N(1)—H(1 N) bond angle. Except the mentioned geometric parameters due to intermolecular hydrogen bonding between the N—hydrogen and the one of the sulfonyl oxygen (N—H···O), the largest difference between experimental and theoretical values was found to be 0.027 Å for bond lengths and 2.6° for bond angles. Possible differences could be due to the fact that while experimental findings in the solid phase were obtained at very low temperature and so the molecular rotations were restricted, the theoretical results were obtained for a single molecule in the gas phase without any intermolecular interactions. As a result, the optimized geometric parameters

Table 2
The experimental bond lengths (Å), bond and torsion angles (°) together within the calculated data for mtsen.

Bond lengths (Å)	Experimental	B3LYP/6-311G(d,p)
S—O(2)	1.432 (2)	1.459
S—O(1)	1.437(2)	1.461
S—N(1)	1.623(2)	1.694
S—C(6)	1.761(2)	1.796
N(1)—C(8)	1.470(2)	1.468
C(7)—C(6)	1.384(3)	1.389
C(7)—C(2)	1.390(3)	1.394
C(6)—C(5)	1.393(3)	1.394
C(8)—C(8)	1.509(3)	1.527
C(2)—C(3)	1.392(3)	1.402
C(2)—C(1)	1.500(4)	1.509
C(5)—C(4)	1.377(3)	1.394
C(4)—C(3)	1.377(3)	1.390
Bond angles (°)		
O(2)—S—O(1)	119.2(1)	121.2
O(2)—S—N(1)	106.0(1)	104.3
O(2)—S—C(6)	109.1(1)	109.5
O(1)—S—N(1)	108.0(1)	110.6
O(1)—S—C(6)	106.5(1)	107.4
S—N(1)—C(8)	118.6(1)	117.6
S—N(1)—H(1 N)	115.4(1)	107.0
C(8)—N(1)—H(1 N)	113.0(2)	114.1
C(6)—C(7)—C(2)	119.9(2)	119.9
S—C(6)—C(7)	118.8(2)	118.8
S—C(6)—C(5)	119.6(2)	119.2
C(7)—C(6)—C(5)	121.7(2)	121.9
N(1)—C(8)—C(8)	109.6(2)	109.0
C(7)—C(2)—C(3)	118.1(2)	118.2
C(7)—C(2)—C(1)	120.0(2)	120.9
C(3)—C(2)—C(1)	121.9(2)	120.7
C(6)—C(5)—C(4)	118.1(2)	118.2
H(009)—C(5)—C(4)	120.9(2)	121.7
C(5)—C(4)—C(3)	120.6(2)	120.3
C(2)—C(3)—C(4)	121.6(2)	121.4
Torsion angles (°)		
O(2)—S—N(1)—C(8)	168.4	161.3
O(2)—S—N(1)—H(1 N)	29.7	31.2
O(2)—S—C(6)—C(7)	31.6	37.8
O(2)—S—C(6)—C(5)	−150.5	−141.4
O(1)—S—C(6)—C(7)	161.5	171.2
N(1)—S—C(6)—C(7	−82.9	−72.3
N(1)—S—C(6)—C(5)	95.0	108.5

obtained at B3LYP/6-311G(d,p) show excellent agreement with the experimental values.

3.3. Vibrational spectral analysis

Mtsen consists of 44 atoms, so it has 126 normal vibrational modes and it is belong to the point group C_1 with only identity (E) symmetry operation. It is difficult to offer an explanation for the vibrational assignments of title compound in the observed vibrational spectra due to its low symmetry. Hence, the assignment of bands was made taking into consideration the literature data for compounds containing appropriate structural fragments [18–20,22,44–53]. All the experimental and theoretical vibrational data are tabulated in Table 3; see also Table S2 (Supporting information) for the description of all vibrational modes. The experimental FT-IR, dispersive Raman spectra of mtsen and comparison with the calculated spectra are given in Figs. 4 and 5. The far-infrared spectrum is also presented in Fig. 6.

3.3.1. N—H vibrations

The N—H stretching vibration of secondary amine groups of some aliphatic or aryl sulfonamides occurs in the region 3300–3200 cm^{-1} [15,44,45]. The strong bands at 3238 cm^{-1} (FT-IR) and 3241 cm^{-1} (Raman) are assigned to the N—H stretching mode of mtsen. On the other hand, this strong mode is split in the Raman spectrum of crystalline mtsen with weak intensity at 3294 cm^{-1} and 3239 cm^{-1}.

The N—H in-plane bending vibration is expected near 1400 cm^{-1} [15,18,20,44,47–49]. This vibration is usually masked by the strong intense band of CH_3 asymmetric bending or SO_2 asymmetric stretching. However, weak intense infrared active bands at 1419 cm^{-1} and 1379 cm^{-1} are assigned to N—H in-plane bending vibration due to having with more contribution according to PED results of related modes.

The calculated PED contribution (γN—H; 27%) and infrared intensity of mode 36 suggest that sole infrared active medium band in Nujol at 644 cm^{-1} is the fundamental band of out-of-plane bending vibration of N—H. But this band is masked by C—S stretching vibration in the FT-IR spectrum of crystalline mtsen. This fundamental band is also observed above 600 cm^{-1} with respect to relevant literature data [18,20,45,49]. Another N—H out-of-pane bending mode, both infrared and Raman active, is observed between 523 cm^{-1} and 527 cm^{-1}.

The splitting wavenumber differences between experimental N—H vibrational bands are around 40–129 cm^{-1}. These downward shifts offer that there is intermolecular hydrogen bonding by the NH moiety of mtsen.

3.3.2. C—H vibrations

The hetero aromatic structures show the presence of C—H stretching vibrations in the region 3100–3000 cm^{-1} which is the characteristic region for the ready identification of C—H stretching vibrations. In this region, the bands are not affected appreciably by the nature of substituents [54–56]. The modes 123 and 119 are due to C—H stretching of hydrogen bonded carbon atoms of phenyl ring. These modes are pure C—H stretching vibrations contributing nearly 100% from the PED results.

The aromatic C—H in-plane bending modes of benzene and its derivatives are observed in the region 1300–1000 cm^{-1} with a weak intensity in the vibrational spectra [54,56]. The C—H out-of-plane bending vibrations occur in the range 1000–750 cm^{-1} in the aromatic compounds [54,56]. The sole infrared active bands observed at 760 cm^{-1} are assigned to aryl C—H out-of-plane bending vibrations from the pure PED outcomes of modes 47. The computations suggest that the expected other bands of C—H in-plane or out-of plane bending vibrations are masked by other strong vibrational modes.

The C—H asymmetric stretching vibrations of the CH_3 group are seen between 2975 cm^{-1} and 2936 cm^{-1}, while the Raman active C—H symmetric band is located around 2928 cm^{-1}. The symmetric alkyl C—H stretching band of the CH_2 group is observed around 2888 cm^{-1} with weak intensity. The other fundamental CH_3 and CH_2 group vibrations which are asymmetric or symmetric CH_3 bending, CH_2 wagging, CH_2 twisting, CH_3 rocking and CH_2 rocking appear in the expected wavenumber region of 1459–760 cm^{-1}.

3.3.3. C—C vibrations

The aromatic carbon–carbon stretching vibration occurs in the region 1625–1430 cm^{-1}. In general, the bands are of variable intensity and observed at 1468–1583, 1625–1590, 1590–1575, 1540–1470, 1460–1430 and 1380–1280 cm^{-1} from the wavenumber ranges given by Varsanyi [56] for the five bands in the region. In the present work, the wavenumbers observed in the FT-IR spectrum at 1603, 1563, 1470, 1223 cm^{-1} and in the Raman spectrum at 1598, 1580, 1222 cm^{-1} were assigned to aromatic C—C stretching vibrations.

3.3.4. S═O vibrations

The SO_2 asymmetric and symmetric stretching vibrations appear in the range 1330 ± 30 cm^{-1} and 1160 ± 30 cm^{-1}, both with high intensity [57,58]. The most intense signals appearing at 1332 cm^{-1} and 1326 cm^{-1} (IR) and the weak intense signal at 1314 cm^{-1} (Ra) are attributed to the SO_2 asymmetric modes. The symmetric νSO_2 stretching vibration is observed at 1151 cm^{-1}. The splitting of the νSO_2 asymmetric bands could be attributed crystal or solid state effects [18,23,49].

The SO_2 scissoring and wagging vibrations occur in the range 570 ± 60 cm^{-1} and 520 ± 40 cm^{-1} [57]. The corresponding bands are observed 587 cm^{-1} and 468 cm^{-1} in the FT-IR spectrum, respectively. The infrared active band at 230 cm^{-1} and Raman active band 229 cm^{-1} are attributed to the SO_2 twisting vibrations from the PED results of modes 19 and 18.

3.3.5. S—N and C—S vibrations

The S—N stretching vibration exhibits a moderate band in the range 905 ± 70 cm^{-1} [57]. This vibration typically occurs a medium band in the IR spectrum and a weak band in the Raman spectrum [57,58]. The infrared studies of some methanesulfonamide [46], arylsulfonamides [44] and n-(substituted phenyl)-methanesulfonamides derivatives [45] are also assigned in the region of 940–836 cm^{-1}, 924–906 cm^{-1} and 926–833 cm^{-1}. The bands at 890 cm^{-1} (IR), 889 cm^{-1} (Raman) and the other at 799 cm^{-1} (IR) are attributed to S—N stretching modes.

The assignment of the band correspond to C—S stretching vibrations in different compounds is difficult. However, νCS band of some methanesulfonamide [46] and n-(substituted phenyl)-methanesulfonamides [45] derivatives in solid phase have been recognized in the region 789–740 cm^{-1}. The calculations suggest that this fundamental band is masked by CH_2 rocking mode. However, the PED result of mode 43, the medium intense infrared active band observed at 664 cm^{-1} is attributed to νCS vibration.

3.3.6. C—N vibrations

The assignments of the CN stretching wavenumbers were made straightforwardly from analogy with 1,2-diaminoethane [51–53]. The vibrational results from pertinent references, the bands between 878 and 1100 cm^{-1} are commonly ascribed to the conformers of 1,2-diaminoethane displaying a gauche orientation around the NCCN dihedral angle [51,53]. However, Batista de Carvalho et al. [53] are reported the band above 1100 cm^{-1} in the Raman spectrum of 1,2-diaminoethane (in solid phase) which confirms

Table 3
The vibrational assignments of the mtsen molecule by normal mode analysis based on SQM force field calculations.

Mode	Experimental[a]					B3LYP/6-311G(d,p)			PED (potential energy distributions)[e]
	Assignment	IR(Nujol)	IR(Crystal)	R(Solid)	R(Crystal)	ν^c	I_{IR}^d	I_R^d	Descriptions (%)
126	N—H stretch			no	3294 vw	3258	21.93	752	ν(N1—H) (100)
125	N—H stretch	3238 s	3241 s	3241 s	3239 w	3224	24.91	1624	ν(N1—H) (100)
	$2 \times \nu_{103}$			3155 vw	3155 vw				
123	C—H stretch (aromatic)	3073 vw sh	3073 vw sh			3066	3.71	2182	$\nu_s(\text{C4,5—H})_{R2}$ (99)
119	C—H stretch (aromatic)	3057 mw	3057 w	3063 s	3064 m	3047	12.69	2768	$\nu_{as}(\text{C3,4,5—H})_{R2}$ (98)
114	$C—H_3$ stretch (asym.)	2975 vw[a]	2975 vw	no	2975 w	2976	16.31	1408	$\nu_{as}(CH_3)_{R1}$ (100)
112	$C—H_3$ stretch (asym.)			2966 m	2966 w	2951	15.45	1747	$\nu_{as}(CH_3)_{R2}$ (100)
111	$C—H_3$ stretch (asym.)	2936 w[b]	2936 w			2951	14.91	1670	$\nu_{as}(CH_3)_{R1}$ (97)
110	$C—H_3$ stretch (sym.)	2927 w sh[b]	2927 w sh			2900	20.81	4175	$\nu_s(CH_3)_{R1}$ (100)
109	$C—H_3$ stretch (sym.)			2926 s	2928 m	2898	20.31	4545	$\nu_s(CH_3)_{R2}$ (100)
108	$C—H_2$ stretch (sym.)	2888 w[b]	2888 w	2887 w sh	2889 w sh	2883	30.59	1699	$\nu_s(\text{C8—H}_2)$ (100)
107	$C—H_2$ stretch (sym.) or $\nu_{97} + \nu_{93}$	2872 w[b]	2872 w			2851	35.18	1263	$\nu_s(\text{C8—H}_2)$ (97)
105	C═C stretch	1603 vw	1603 w	1601 w	1598 w	1620	10.08	1054	$\nu(CC)_{R2}$ (78)
103	C═C stretch	1577 vw	1563 w	1578 w	1580 w	1596	0.47	1153	$\nu(CC)_{R2}$ (80)
100	C═C stretch	1469 s[b]	1470 s			1478	17.01	227	$\nu(CC)_{R2}$ (49) + $\delta(CH)_{R2}$ (37)
97	$C—H_3$ bend (asym.)	1454 s[b]	1454 s			1450	17.44	302	$\delta_{as}(CH_3)_{R2}$ (67) + $\nu(\text{C6—C7})_{R2}$ (6)
96	$C—H_3$ bend (asym.)			1458 w	1459 vw	1441	7.14	738	$\delta_{as}(CH_3)_{R2}$ (99)
93	N—H bend (ip.)	1419 w[b]	1419 w			1418	25.89	266	δ(N1—H) (33) + $\nu_{as}(\text{C3,6—C4,7})_{R2}$ (9) + $\nu_{as}(\text{S1—O}_2)$ (8) + $\delta_{as}(CH_3)_{R2}$ (7)
91	N—H bend (ip.)	1379 w[b]	1379 w			1403	75.72	257	δ(NH) (49) + $\omega(\text{C8—H}_2)$ (22)
90	CH_2 wag			1377 m	1378 w	1381	1.40	957	$\omega(CH_2)$ (45) + δ(N1—H) (15)
87	$S—O_2$ stretch (asym.)	1332 vs[b]	1332 vs			1342	7.31	205	$\nu_{as}(\text{S—O}_2)$ (69)
84	$S—O_2$ stretch (asym.)	1326 vs[b]	1326 vs	1313 w	1314 w	1321	152.49	382	$\nu_{as}(\text{S—O}_2)$ (61) + $\nu(CC)_{R1}$ (23)
80	CH_3 bend (sym.)	1304 vs[b]	1304 vs			1277	90.09	97	umb(CH_3) (35) + $\omega(\text{C—H})_{methylene}$ (25) + δ(NH) (7)
79	$C—CH_3$ stretch	1223 m	1223 m			1215	7.71	492	$\nu_{as}(\text{C2—CH}_3)$ (32) + $\delta(\text{C3,7—H})_{R2}$ (15) + $\nu_s(\text{C3—C2—C7})_{R2}$ (12)
78	$C—CH_3$ stretch			1222 m	1222 m	1214	4.88	1475	$\nu_{as}(\text{C2—CH}_3)$ (32) + $\nu_s(\text{C3—C2—C7})_{R1}$ (16) + $\delta(\text{C3,7—H})_{R1}$ (15)
77	$C—H_2$ twist	1176 m	1176 m sh	1172 m	1171 w	1195	3.76	263	tw(CH_2) (72) + δ(NH) (11)
74	$S—O_2$ stretch (sym.)			1151 m	1151 m	1142	93.74	1712	$\nu_s(\text{S—O}_2)$ (81)
73	$S—O_2$ stretch (sym.)	1152 vs	1151 vs			1133	233.37	229	$\nu_s(\text{S—O}_2)$ (79)
70	C—N stretch	1100 m	1100 s	1111 m	1110 w	1098	23.12	419	ν_s(CN) (72) + δ_s(CCN) (7)
68	C═C═C stretch (sym.)	1088 s	1088 s			1081	45.01	374	$\nu_s(CCC)_{ar}$ (41) + $\delta(\text{C7—H})_{ar}$ (13) + $\nu_s(\text{S—O}_2)$ (8) + ν(C8—N1) (5)
66	C—N stretch	1065 vs	1065 vs	1060 w	1059 vw	1069	118.56	1308	ν_{as}(CN) (67) + $\nu(CC)_{methylene}$ (4)
62	$C—H_3$ rock	997 w	996 m			994	5.67	2038	$\rho(CH_3)_{R1}$ (68) + $\nu_s(\text{C2—C3—C4})_{R1}$ (11)
61	$C—H_3$ rock			999 vs	999 vs	991	2.57	2920	$\rho(CH_3)_{R2}$ (68) + $\nu_s(\text{C2—C3—C4})_{R2}$ (11)
56	C—H bend (op./aromatic)	932 w	933 w			923	0.33	100	$\gamma(CH)_{R2}$ (90)
52	S—N stretch	890 s	890 s	891 m	889 w	883	67.91	2529	ν_s(SN) (36) + $\nu(\text{C2—CH}_3)_{R1}$ (7) + ν(C6—S) (7) + $\nu(CC)_{methylene}$ (5)
51	$C—CH_3$ stretch	860 w	852 w	857 w		859	56.37	720	$\nu_s(\text{C2—CH}_3)_{ar}$ (23) + $\nu_s(\text{C3—C2—C7})_{R2}$ (12) + ν_{as}(CS) (16) + ν(S—N1) (8)
50	$C—CH_3$ stretch				834 vw	842	9.77	487	$\nu_s(\text{C2—CH}_3)_{ar}$ (19) + ν_s(CS) (16) + ν_s(SN) (13) + $\nu_s(\text{C3—C2—C7})_{R2}$ (8)
49	S—N stretch	792 m	799 w sh			807	112.33	236	ν_{as}(SN) (33) + $\rho(\text{C8—H}_2)$ (12) + $\nu(\text{C2—CH}_3)_{R1}$ (4)
48	$C—H_2$ rock	785 m	782 m	no	785 vw	794	89.10	1098	$\rho(CH_2)$ (56) + ν(S—N1) (23)
47	C—H bend (op./aromatic)	763 w	760 w			788	31.44	274	$\gamma(\text{C3,4,5—H})_{R2}$ (85)
45	C═C═C bend (op.)	693 s	692 vs	694 s	695 m	692	38.24	1209	$\gamma(CCC)_{R2}$ (80)
43	C—S stretch	656 m	664 m			683	25.92	224	ν(C6—S) (34) + $\gamma(CCC)_{R2}$ (29) + $\nu(\text{C2—CH}_3)_{R2}$ (5)
41	N—H bend (op.)	no	644 m			621	57.20	2507	γ(N1—H) (27) + sci(S—O_2) (19) + ν(S—N1) (15)
40	$S—O_2$ scissor	585 s	587 vs	593 w	595 w	595	342.74	619	sci(S—O_2) (38) + γ(N1—H) (23)
39	C—S—N bend (op., asym.)			574 w	575 w	579	17.49	307	γ_{as}(C6—S—N1) (36) + $\gamma(CCC)_{R1}$ (3)
36	N—H bend (op.)	527 w	527 w	523 m	525 w	533	88.20	886	γ(N1—H) (29) + $\omega(\text{S—O}_2)$ (14) + $\gamma(CCC)_{R1}$ (8) + $\nu(\text{C2—CH}_3)_{R1}$ (3)
34	C═C═C bend (ip., sym.)	515 vw	513 w	490 vw	485 vw	510	49.09	1040	$\delta_s(CCC)_{R1}$ (50) + $\nu(\text{C2—CH}_3)_{R1}$ (22)
33	SO_2 wag	467 s	468 s			488	21.76	117	$\omega(SO_2)$ (38) + δ_{as}(CCN) (12)
30	O═S—N bend (ip., asym.)	441 vw	441 vw			447	29.93	257	δ_{as}(O1SN) (12) + $\tau(CC)_{R2}$ (8) + ν(S—N1) (4)
27	Ring-CH_3 bend (ip.)	414 w	414 w	417 w	421 vw	392	0.94	333	$\delta(\text{C}_{ar}\text{—CH}_3)_{R1}$ (33) + tw(SO_2) (15)
26	Ring-CH_3 bend (ip.)	374 w				385	12.16	166	$\delta(\text{C}_{ar}\text{—CH}_3)_{R2}$ (26) + δ_s(O1SN) (10) + ν(C6—S) (3)
24	Ring-CH_3 bend (ip.)			336 w	331 w	318	0.91	916	$\delta(\text{C}_{ar}\text{—CH}_3)_{R2}$ (24) + ν(C6—S1) (17) + δ_s(O2SC6) (14) + τ(C8—N1) (12)
23	C—S—N bend (op., asym.)	309 m		300 w	300 w	309	0.94	1033	γ_{as}(C6—S—N1) (34) + ν(C6—S) (21) + $\delta(\text{C}_{ar}\text{—CH}_3)_{R2}$ (15)
19	$S—O_2$ twist	230 vw				244	2.77	596	tw(S—O_2) (30) + ω(CCN) (12) + ν(C6—S1) (6)
18	$S—O_2$ twist			229 vs	229 m	212	1.29	1969	tw(SO_2) (27) + γ_s(CCN) (18) + ν_s(CN) (13) + ν_s(SN) (13)
15	C—C torsion			161 m	155 vw	168	0.60	1498	$\tau(CC)_{methylene}$ (28) + τ(S—N1) (17)
11	SO_2–Ring torsion	127 w		no	133 w	131	2.23	4635	$\tau(SO_2\text{-ring})$ (43) + τ(C8—N1—S1) (10)

(continued on next page)

Table 3 (*continued*)

Mode	Experimental[a]					B3LYP/6-311G(d,p)			PED (potential energy distributions)[e]
	Assignment	IR(Nujol)	IR(Crystal)	R(Solid)	R(Crystal)	ν[c]	I_{IR}[d]	I_R[d]	Descriptions (%)
10	C—N—S torsion	89 w				93	2.12	1507	τ(CNS) (42) + τ(SO_2-R1) (9) + τ(CC) (4)
9	C—N—S torsion	80 w sh				83	2.03	1431	τ(C8—N1—S) (21) + τ(SO_2-R2) (16) + τ(C6—S—N1) (11) + τ(CCN) (8)
8	C—C—N torsion	58 w				64	4.51	493	τ(CCN) (56) + τ(CNS) (20)
6	C—H_3 torsion	35 vw				31	0.35	2781	τ$(CH_3)_{R2}$ (95)

[a] vs: very strong, s: strong, m: medium, w: weak, vw: very weak, sh: shoulder, br: broad, no: not observed, asym.: asymmetric, sym.: symmetric, ip.: in-plane, op.: out-of-plane and IR: infrared and R: Raman.
[b] The infrared active vibrational wavenumbers are obtained in hexachloro-1,3-butadiene.
[c] Wavenumbers scaled by SQM FF methodology according to our scale factors (See the text).
[d] I: intensity, IR: infrared and R: Raman. The relative intensities of the simulated spectra were obtained after using the pure Lorenzian band shapes with a band with 10 cm^{-1}.
[e] R1: ring1, R2: ring2, ar: aromatic, ν: bond stretching, δ: in-plane angle bending, γ: out-of-plane angle bending, umb: umbrella bending, sci: scissoring, tw: twisting, ω: wagging, ρ: rocking, τ: torsion, as: asymmetric and s: symmetric. PED less than 3% are not shown.

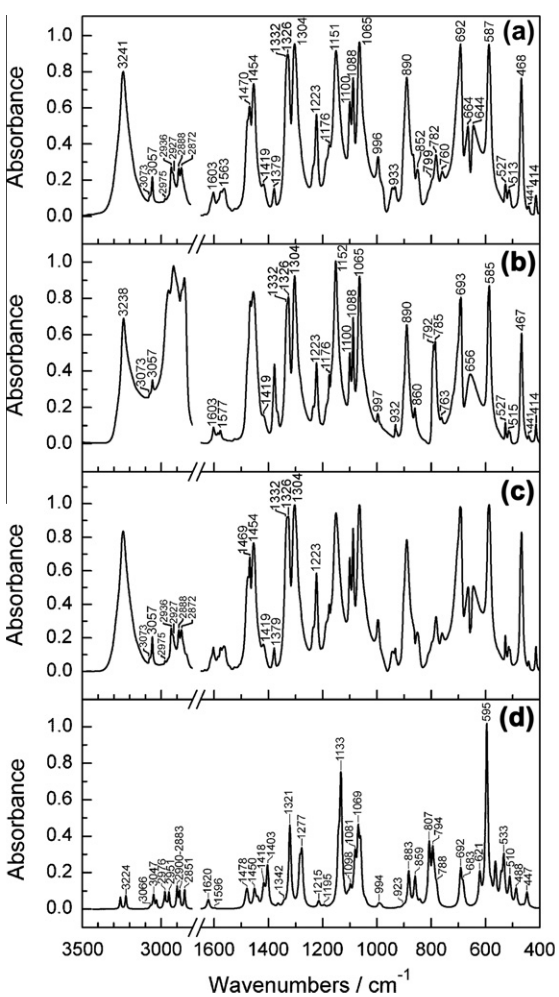

Fig. 4. The FT-IR spectra of mtsen: (a) single crystalline, (b) in Nujol, (c) in hexacholoro-1,3-butadiene and (d) calculated.

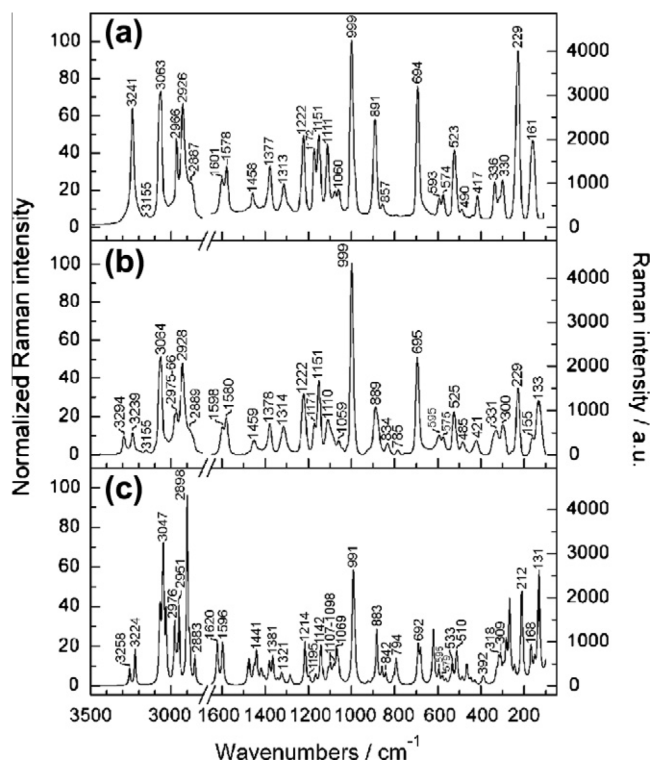

Fig. 5. The dispersive Raman spectra of mtsen: (a) non-crystalline, (b) single crystalline and (c) calculated.

the trans skeletal arrangement around the C—C axe. Hence, in the present investigation, the bands at 1100 and 1065 cm^{-1} (IR), 1110 and 1059 cm^{-1} (Ra) is assigned to the fundamental C—N stretching.

3.3.7. Skeletal vibrations

The low wavenumber region generally gives more qualified information about the conformational behaviors of the compounds [23,26,53]. Computational wavenumbers in this region (below 600 cm^{-1}) are sensitive than high wavenumber region. As clearly seen from Table 3, the computed wavenumbers are great agreement with the experimental ones. This agreement tends to us make more reliable vibrational assignment of title compound. The skeletal vibrations, such as O—S—N asymmetric in-plane bending, ring-CH_3 in-plane bending, SO_2 twist and torsional vibrations are undoubtedly assigned.

3.4. Comparison of the characteristic vibrations of the ligand and complex

Infrared spectra support the structure of the [Cu(phen)$_2$]L complex by the determination of the coordination modes. The changes in the characteristic vibrations of the ligand were compared with complex. Before comparison, the experimental FT-IR spectrum of [Cu(phen)$_2$]L is given in Fig. 7.

The strong intense υNH band of free ligand was observed around 3238 cm^{-1} in Nujol solution and 3241 cm^{-1} in crystalline phase, but

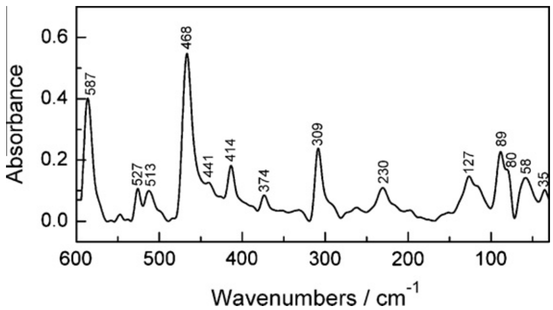

Fig. 6. The far-infrared spectrum of mtsen.

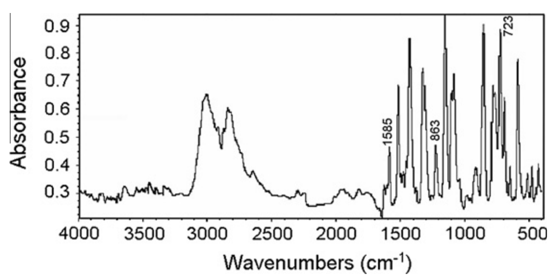

Fig. 7. The FT-IR spectrum of $[Cu(phen)_2]L$.

Table 4
The experimental ^{13}C and ^{1}H NMR chemical shifts (ppm) together within the calculated data for mtsen in DMSO-d_6.

Assignment	Experimental[a]	B3LYP/6311++G(d,p)[b]
C6	140.15	143.80
C2	138.89	140.96
C3	133.04	134.47
C4	129.03	130.01
C7	126.60	127.11
C5	123.53	123.49
C8	42.20	42.71
C1	20.80	20.36
H—C7	7.55 s	7.91
H—C5	7.51 d	7.85
H—C3	7.49 s	7.74
H—C4	7.46 d	7.73
H—N1	7.64 s	4.34
H_2—C8	2.74 s	2.66
H_3—C1	2.38 s	2.46

[a] s: Singlet and d: doublet.
[b] σ Transform into δ using equations given in Ref. [23]; $\delta^{13}C = 175.7–0.963\ \sigma^{13}C$ and $\delta^{1}H = 31.0–0.970\ \sigma^{1}H$.

it disappeared by the chelation through the amide nitrogen in the complex. This observation indicates deprotonation of the amide group. The asymmetric and symmetric SO_2 bands did not show significant shifts with respect to those of ligand, in spite of deprotonation of the amide group [36–43]. In the FT-IR spectra of the complex the vibration of the imine nitrogen bond (C═N) of the stretching band of the phenanthroline rings shifts from 1644 cm^{-1} to 1585 cm^{-1} by the complexation which causes a great need for the oscillation of the bonds in the ring. And as the electron clouds of the C—N bonds flow to the phenanthroline rings, making the electron density around the C—N bonds decreased, the stretching vibration of the C—N bond in complex shifts to low wavenumber region. And also, the C—H out-of-plane bending vibrations of the phenanthroline ring were shifted in the 855 cm^{-1} and 715 cm^{-1} as compared with coordination compound in the 863 cm^{-1} and 723 cm^{-1} because of due to take part in between ligand and Cu(II) [36,59].

3.5. NMR spectra

The experimental ^{13}C and ^{1}H NMR chemical shifts (ppm) together within the calculated data for mtsen in DMSO-d_6 are given in Table 4. It is well-known that symmetric C and H atoms in the compounds show the same chemical shift due to having same chemical environment. Considering the chemical environment, mtsen shows eight different carbon atoms in ^{13}C NMR spectrum (Fig. 8a). The two peaks observed at 42.20 ppm and 20.80 ppm are attributed to protons of H_2—C8 and H_3—C1, respectively. The other six peaks between 140.15 ppm and 123.53 ppm are assigned to aromatic carbon protons. In Fig. 8b, aromatic proton peaks were also observed at about 7.54–7.46 ppm. The experimental N—H protons shift (4.34 ppm) showed poor correlation with the calculated proton shifts (7.64 ppm). The reason of this correlation is the N—H protons have intra- or intermolecular hydrogen bonding [23]. The Heteronuclear Chemical-Shift Correlation (HETCOR) and Correlation Spectroscopy (COSY) spectrum of mtsen in Fig. 8c and d were also confirmed the ^{1}H NMR spectrum.

3.6. Antibacterial bioassay

Mtsen and $[Cu(phen)_2]L$ compounds were screened in vitro for their antibacterial activity against three Gram-negative (*Escherichia coli*, *P. aeruginosa* and *Y. enterocolitica*) and three Gram-positive species (*S. aureus*, *Bacillus subtilis* and *Bacillus cereus*) of bacterial strains by the microdilution and agar-disk diffusion method. The antimicrobial activity of mtsen and $[Cu(phen)_2]L$ compounds with dilution method are tabulated in Table 5. As seen from the table, compounds showed overall a remarkable activity against *E. coli, Y. enterocolitica, B. cereus and S. aureus* bacterial strains. In addition, $[Cu(phen)_2]L$ compound shows higher antibacterial activity than ligand molecule. The highest activity with the lowest MIC value of $[Cu(phen)_2]L$ compound is against the Gram negative bacteria *E. Coli* and *Y. enterocolitica*.

The inhibition zones formed by standard antibiotics (*ciprofloxacin, Penicillin and Ampicillin*) against all bacteria are reported in Table 6. The results were compared with those of the standard drugs. All compounds exhibited significant activity than *Penicillin* and *Ampicillin* for all Gram-negative and Gram-positive bacterial strains.

4. Conclusion

In the present work, we were performed experimental and theoretical vibrational, NMR and XRD analyses of msen, for the first time. The molecular geometric parameters, vibrational wavenumbers, infrared and Raman intensities of the title molecule in the ground state were calculated by using B3LYP method with 6-311G(d,p) basis set. A complete vibrational analysis was also performed according to our frequency scale factors which were firstly used in our last study within the SQM-FF method based on the same theory level. The great match between experimental and calculated vibrational wavenumbers and intensities of each vibrational mode enables us to safely assign the fundamental bands. Some fundamental bands in the vibrational spectra such as N—H in-plane bending, SO_2 asymmetric stretching, C—N stretching, S—N stretching and N—H out-of-plane bending bands are split, which can be attributed to solid state effects or caused by the intermolecular hydrogen bonding between the N—hydrogen and the one of the sulfonyl oxygen. To confirm the hydrogen bonding in liquid state, ^{1}H and ^{13}C chemical shifts were calculated at B3LYP/6-311++G(d,p) theory level and were compared with experimental values. The observed and the calculated isotropic chemical shifts are found to be in good agreement with the exception of N—H protons shift. The reason of this discrepancy can be shown due to the intermolecular hydrogen bonding.

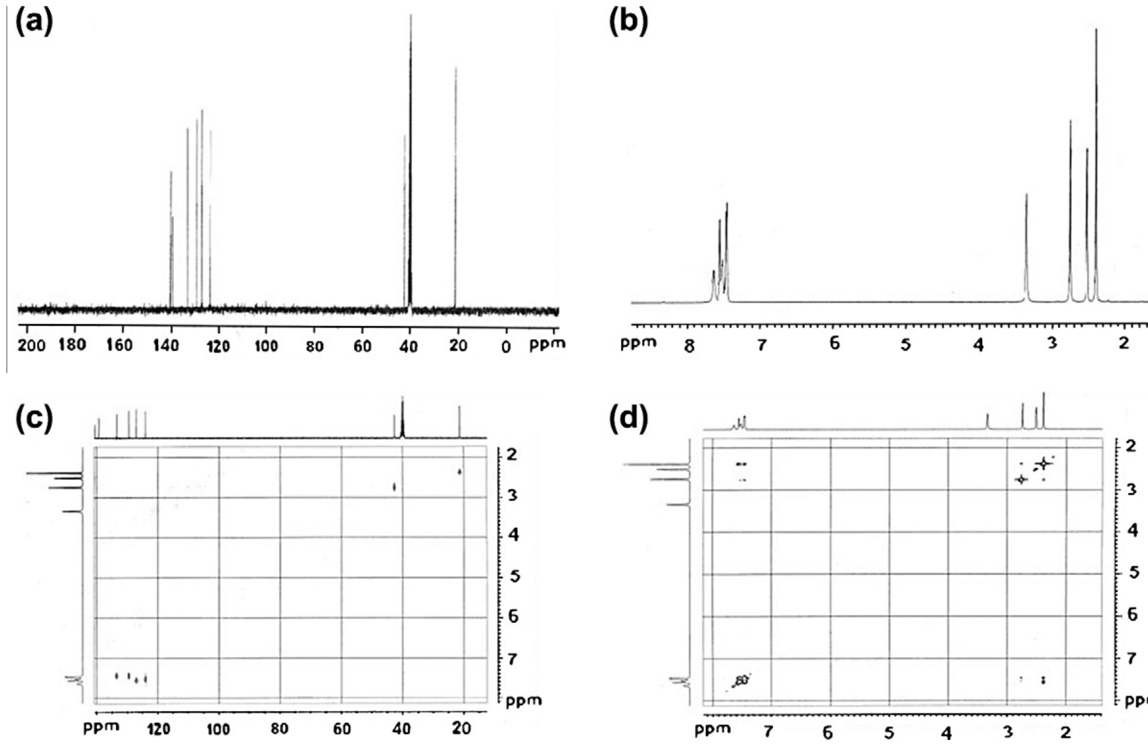

Fig. 8. The NMR spectra of mtsen in DMSO-d_6: (a) ^{13}C, (b) ^{1}H, (c) HETCOR and (d) COSY.

Table 5
Antimicrobial activity of mtsen and its Cu(II) complex with microdilution method.

Compound	*MIC* (μg/mL)					
	Escherichia coli ATCC 35218	*P. aeruginosa ATCC 27853*	*Y. enterocolitica O:3*	*Bacillus cereus RSKK 709*	*Bacillus subtilis ATCC 6633*	*S. aureus ATCC 25923*
mtsen	80	120	80	80	240	100
$[Cu(phen)_2]L$	60	100	60	80	120	80

Table 6
Result of the antimicrobial test of mtsen and its Cu(II) complex disk potency 70 μg.

Compound	Diameter inhibition zone (mm, 70 μg/disk)					
	Escherichia coli ATCC 35218	*P. aeruginosa ATCC 27853*	*Y. enterocolitica :3*	*Bacillus cereus RSKK 709*	*Bacillus subtilis ATCC 6633*	*S. aureus ATCC 25923*
mtsen	23	24	18	16	20	18
$[Cu(phen)_2]L$	25	26	20	22	23	20
Ciprofloxacin	36	–	–	26	–	29
Penicillin	17	–	–	8	–	8
Ampicillin	11	–	–	13	–	14

<10: Weak; >10: moderate; >16: significant.

Further analyses were also made for $[Cu(phen)_2]L$ complex by using elemental analysis, LC–MS, magnetic susceptibility; conductivity measurement and FT-IR. The comparison of the characteristic experimental vibrations of the ligand and complex along with the structural agreement from the magnetic susceptibility and conductivity measurement data led us to understand the molecular structure and coordination about the complex. The structure of complex is proposed as a tetragonal geometry.

The biological activity of two compounds screening indicated that complex has more activity than ligand against the tested bacteria. However, two compounds exhibited significant activity than standard antibiotic drugs Penicillin or Ampicillin.

Appendix A. Supplementary material

Supplementary data associated with this article can be found, in the online version, at http://dx.doi.org/10.1016/j.molstruc.2012.06. 046.

References

[1] N. Anand, Burger's medicinal chemistry and drug discovery, in: M.E. Wolff (Ed.), Therapeutic Agents, 5th ed., J. Wiley & Sons, New York, 1996.
[2] A. Mastrolorenzo, A. Scozzafava, C.T. Supuran, Eur. J. Pharm. Sci. 11 (2000) 99.
[3] E.R. Barnhart (Ed.), Physicians Desk Reference, PDR, 43rd ed., Medical Economics, New York, 1989.
[4] H. Singh, V.K. Srivastava, S.N. Shukla, M.K. Srivastava, M.K. Upadhyay, Indian J.

Chem. 33A (1994) 350.
[5] K.A. Metwally, L.M. Abdel-Aziz, E.M. Lashine, M.I. Husseiny, R.H. Badawy, Med. Chem. 14 (2006) 8675.
[6] N. Hadj-esfandiari, L. Navidpour, H. Shadnia, M. Amini, N. Samadi, M.A. Faramarzi, A. Shafiee, Bioorg. Med. Chem. Lett. 17 (2007) 6354.
[7] M.W. Khan, M.J. Alam, M.A. Rashid, R. Chowdhury, Bioorg. Med. Chem. 13 (2005) 4796.
[8] Z. Nilo, Med. Chem. 15 (2007) 1947.
[9] R.A. Greenfield, M.S. Bronze, Drug Discov. 8 (2003) 881.
[10] W. Martindale, in: J.E.F. Reynolds (Ed.), The Extra Pharmacopoeia, 31st ed., Royal Pharmaceutical Society, London, 1996.
[11] A. Bult, in: H. Siegel (Ed.), Metal Ions in Biological Systems, Marcel Dekker, New York, 1983. Chapter 16.
[12] S.C. Chaturvedi, S.H. Mishra, K.L. Bhargava, Sci. Cult. 46 (1980) 401.
[13] F. Blasco, R. Ortiz, J. Inorg. Biochem. 53 (1994) 117.
[14] S. Alyar, N. Karacan, J. Enzy, Inhib. Med. Chem. 24 (2009) 986.
[15] N. Ozbek, H. Katırcıoglu, N. Karacan, T. Baykal, Bioorg. Med. Chem. 15 (2007) 5105.
[16] S. Alyar, N. Ozbek, N. Karacan, Drug Future 32 (2007) 126.
[17] N. Ozbek, S. Alyar, N. Karacan, Drug Future 32 (2007) 128.
[18] A. Ienco, C. Mealli, P. Paoli, N. Dodoff, Z. Kantarci, N. Karacan, New J. Chem. 23 (1999) 1253.
[19] N. Ozbek, S. Alyar, N. Karacan, J. Mol. Struct. 1–3 (2009) 48.
[20] N.I. Dodoff, U. Ozdemir, N. Karacan, M.Ch. Georgieva, S.M. Konstantinov, M.E. Stefanova, Z. Naturforsch. 54b (1999) 1553.
[21] N. Ozbek, G. Kavak, Y. Ozcan, S. Ide, N. Karacan, J. Mol. Struct. 919 (2009) 154.
[22] S. Alyar, U.O. Ozmen, N. Karacan, O.S. Senturk, K.A. Udachin, J. Mol. Struct. 889 (2008) 144.
[23] H. Alyar, A. Ünal, N. Özbek, S. Alyar, N. Karacan, Spectrochim. Acta A 91 (2012) 39.
[24] M.J. Frisch, et al., Gaussian 03 Revision D.01, Gaussian Inc., Wallingford, CT, 2004.
[25] SQM version 1.0, Scaled Quantum Mechanical, 2013 Green Acres Road, Fayetteville, Arkansas 72703.
[26] A. Ünal, M. Şenyel, Ş. Şenturk, Vib. Spectrosc. 50 (2009) 277–284.
[27] G. Keresztury, S. Holly, J. Varga, G. Besenyei, A.Y. Wang, J.R. Durig, Spectrochim. Acta A 49 (1993) 2007.
[28] K. Wolinski, J.F. Hinton, P. Pulay, J. Am. Chem. Soc. 112 (1990) 8251.
[29] J.R. Cheeseman, G.W. Trucks, T.A. Keith, M.J. Frisch, J. Chem. Phys. 104 (1996) 5497.
[30] Rigaku/MSC, Inc., 9009 new Trails Drive, The Woodlands, TX 77381.
[31] G.M. Sheldrick, SHELXS97 and SHELXL97, University of Göttingen, Germany, 1997.
[32] E.W. Koneman, S.D. Allen, W.M. Janda, P.C. Scherckenberger, W.C. Winn, Color Atlas and Textbook of Diagnostic Microbiology, Lippincott-Raven, Philadelphia, 1997.
[33] A.W. Bauer, W.M. Kirby, J.C. Sherris, M. Turck, Am. J. Clin. Pathol. 45 (1966) 493.
[34] E.-M. Zerbe, O. Moers, P.G. Jones, A. Blaschette, Z. Naturforsch. 60b (2005) 125.
[35] G. Ferguson, C. Glidewell, J. Chem. Soc. Perkin Trans. 2 (1988) 2129.
[36] S. Alyar, N. Özbek, N.O. İskeleli,N. Karacan, Med. Chem. Res., http://dx.doi.org/10.1007/s00044-012-0171-2.
[37] W.J. Geary, Coord. Chem. Rev. 7 (1971) 81.
[38] J. Casanova, G. Alzuet, J. Borras, O. Carugo, J. Chem. Soc. Dalton Trans. (1996) 2239.
[39] L. Gutierrez, G. Alzuet, J.A. Real, J. Cano, J. Borras, A. Castineiras, Inorg. Chem. 39 (2000) 3608.
[40] G. Alzuet, J.A. Real, J. Cano, J. Borras, R. Santiago-Garcia, S. Garcia-Granda, Inorg. Chem. 40 (2001) 2420.
[41] J. Casanova, G. Alzuet, S. Ferrer, J. Latorre, J.A. Ramirez, J. Borras, Inorg. Chim. Acta 304 (2000) 170.
[42] L. Gutierrez, G. Alzuet, J. Borras, A. Castineiras, A. Rodriguez-Fortea, E. Ruiz, Inorg. Chem. 40 (2001) 3089.
[43] S. Ferrer, J. Borras, C. Miratvilles, A. Fuertes, Inorg. Chem. 28 (1989) 160.
[44] B.T. Gowda, K. Jyothi, J.J. D'Souza, Z. Naturforsch. 57a (2002) 967.
[45] K.L. Jayalakshmi, B.T. Gowda, Z. Naturforsch. 59a (2004) 491.
[46] Y. Tanaka, Y. Tanaka, Chem. Pharm. Bull. 13 (1965) 858.
[47] K. Hanai, T. Okuda, T. Uno, K. Machida, Spectrochim. Acta A 31 (1975) 1217.
[48] R.D. Bindal, J.T. Golab, J.A. Katzenellenbogen, J. Am. Chem. Soc. 112 (1990) 7861.
[49] N.I. Dodoff, Internet J. Vib. Spec. 3 (1999) 7.
[50] G. Liang, J.P. Bays, J.P. Bowen, J. Mol. Struct. (Theochem) 401 (1997) 165.
[51] Y.L. Yu, H.H. Huang, J. Mol. Struct. 412–483 (1997) 141.
[52] S. Kudoh, M. Takayanagi, M. Nakata, T. Ishibashi, M. Tasumi, J. Mol. Struct. 479 (1999) 41.
[53] L.A.E. Batista De Carvalho, L.E. Lourenco, M.P.M. Marques, J. Mol. Struct. 482–483 (1999) 639.
[54] R.M. Silverstein, G.C. Bassler, T.C. Morrill, Spectrometric Identification of Organic Compounds, Wiley, New York, 1981.
[55] V. Krishnakumar, R. Ramasamy, Spectrochim. Acta A 62 (2005) 570.
[56] G. Varsanyi, Assignments of Vibrational Spectra of 700 Benzene Derivatives, Wiley, New York, 1974.
[57] N.P.G. Roeges, A Guide to the Complete Interpretation of Infrared Spectra of Organic Structures, Wiley, New York, 1994.
[58] R.M. Silverstein, F.X. Webster, Spectrometric Identification of Organic Compounds. 6th ed., Wiley, Asia, 2003.
[59] Z. Yongliang, Z. Fengying, L. Qiang, G.J. Deqing, J. Rare Earth 24 (2006) 18.